International Journal of Mechanical Sciences 168 (2020) 105301

Contents lists available at ScienceDirect

International Journal of Mechanical Sciences

journal homepage: www.elsevier.com/locate/ijmecsci

Effect of temperature difference on the mechanical responses of ribbon kirigami: Toward the highly stretchable conductors

Yafei Wang, Changguo Wang*

National Key Laboratory of Science and Technology for National Defence on Advanced Composites in Special Environments, Harbin Institute of Technology, Harbin 150080, PR China

ARTICLE INFO

Keywords:
Kirigami
Stiffness
Stretchability
Thermal effect
Optimization
Stretchable conductor

ABSTRACT

Kirigami-patterned designs through photolithography technology present a promising set of strategy for highly stretchable conductors, which have been investigated to open up a wide range of novel technological solutions for various applications, such as stretchable bioprobe and wearable thermotherapy. The kirigami-patterned conductors usually suffer steady temperature difference and consequent thermal load, because of the Joule heating effect under input voltages. The concealed relationships between thermal effects, geometric effects and mechanical responses are of great significance for practical applications. Here, a closed-form analytical solution, considering the thermal effect and large curvature curved beam theory, is developed to study the stretchability and stiffness for a class of ribbon kirigami structures. Both of finite element method and experiments are performed to validate the accuracy and scalability of model. Comparisons of the developed closed-form stretchability and stiffness to the model with thermal effect absent present quantitative characteristic towards the thermal effect, the remarkable underestimate of stretchability (e.g., >8% relatively) and overestimate of stiffness (e.g., >5% relatively) can be induced by the thermal-effect-absent model for many representative ribbon kirigami patterns. Moreover, several demonstrations present the capability of developed model in optimization of ribbon-kirigami-patterned conductors under the thermal effect and practical geometry constraint conditions, achieving the most stretchable devices. This study provides the theoretical guide for kirigami-based conductor designs in applications.

1. Introduction

Kirigami, a Japanese art of paper cutting, has recently inspired the design of highly stretchable and morphable devices that can be easily realized by arranging a series of extremely delicate cuts into a 2D sheet made up of advanced materials [1–8]. The kirigami-inspired design strategies hold great potential in a wide of range of applications, from ultrastretchable bioprobes [9], to wearable electronics/thermotherapy [10,11], to diffraction gratings [12], to force sensors [3], to soft deployable reflectors [13], to triboelectric generators [14] and to transparent electronic skin [15]. In order to bridge the vast design space of possible kirigami-inspired metamaterial structures and the desired functionalities of the targeted physical effect, a wide variety of material design paradigms are developed, including the allowable pluripotent materials that root in polyvinylidene difluoride [16], aluminum-doped conductive material [10], magneto elastomer [17], metallic nanowire reinforced nanocomposite [18–20], Kapton/GaAs [21], graphene oxide/PVA [4], Ag/aramid [22] and nanostructured materials (such as carbon nanotubes, nano-crystals, nanowires, 2D materials) [23,24]. Of these paradigms, formation of kirigami-patterned stretchable conductor with high stretchability and stable conductivity presents a promising paradigm [23,24], as illustrated in Fig. 1a, because of the improved portability/biocompatibility with artificial microelectronic systems adapted to the trends in modern electronics, and the highly parallel mechanical-physical responses in kirigami structures and materials over the traditional materials [9–11,15,19,20,25–29]. In particular, the Joule heating effect in kirigami-patterned conductors allows the formation of steady-state temperature difference and consequent thermal load, during the tensile process of conductor with input voltage [4,10,22,24,27,28,30,31]. This integrated system enables the high-precision bioprobes and sensors, etc., in a reversible manner within the elastic regime [3,9,10,12,21,26,28]. The assessment of feasibility and reliability is a great challenge but urgent for those applications, as the errors involving mechanical responses induced by thermal effects (such as hundreds of temperature difference) sometimes are dangerous to high-precision devices, and an analytical model considering thermal effects is required to guide the optimization design to achieve the desired stretchability, stiffness and geometry. Although the theoretical model have been developed to investigate the stretchability and stiffness for specific kirigami patterns (i.e., straight cutting or curved cutting) [7,17,32–37], these studies are mostly on the premise that thermal effects are ignored [10,22,24,27], and it appears that there has been only limited research into mechanical performance of kirigami-patterned structures

* Corresponding author.
E-mail address: wangcg@hit.edu.cn (C. Wang).

https://doi.org/10.1016/j.ijmecsci.2019.105301
Received 18 August 2019; Received in revised form 15 October 2019; Accepted 2 November 2019
Available online 4 November 2019

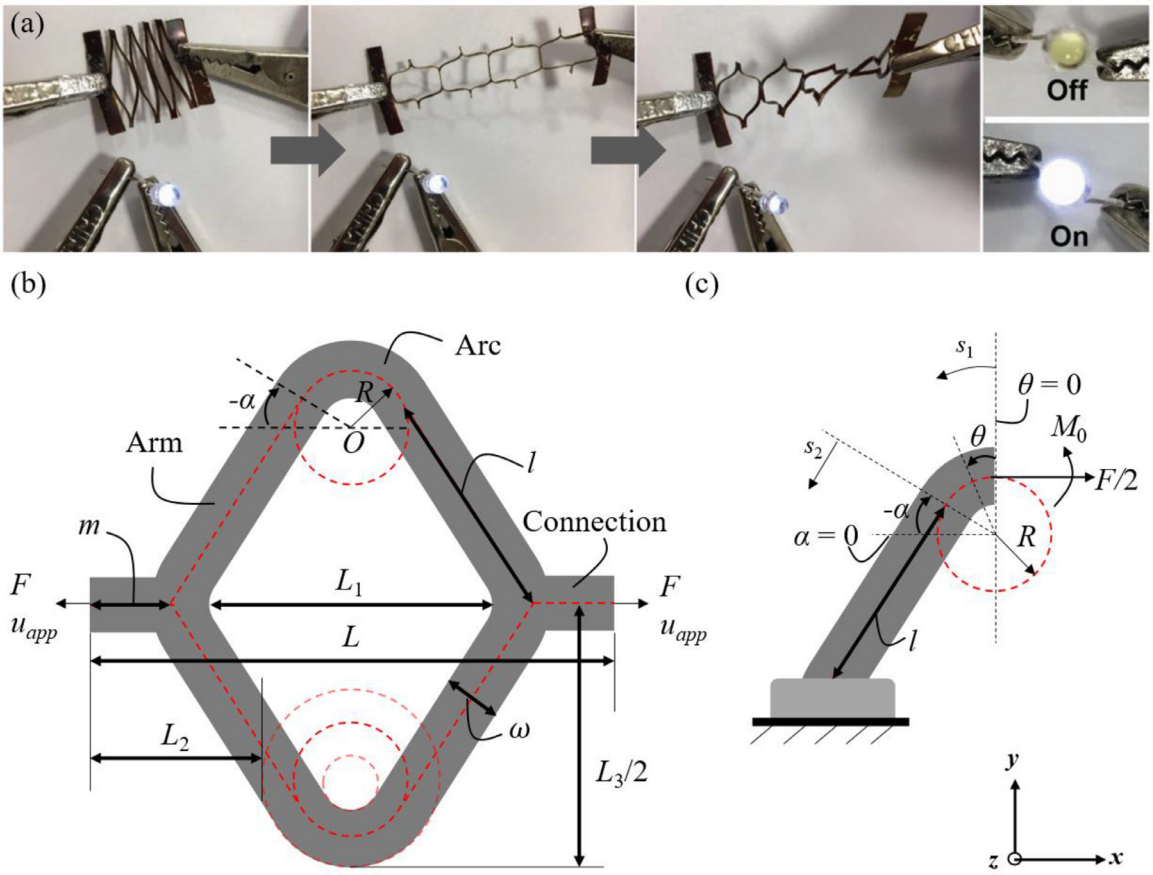

Fig. 1. (a) Schematic illustration of the kirigami-patterned polymer sheet with α= 0 can be highly stretchable as an electrical conductor device to wire LED [24]. (b) Schematic illustration of a representative ribbon kirigami unit cell subjected to an axial tensile displacement u_{app} at two ends. (c) Schematic illustration of the simplified model for the ribbon kirigami unit cell.

under the action of thermal effects (or loads). Especially, the previous theories cannot be directly used to investigate the optimization problem of kirigami-patterned structures with the most stretchability under the condition of thermal effects and practical geometry constraints. In this paper, a closed-form analytical solution based on the consideration of thermal effects and large curvature curved beam (LCCB) theory is developed to predict the stretchability and stiffness of ribbon kirigami with thermal loads. The underlying relationships between thermal effects, geometric effects and mechanical responses are unveiled. Accuracy and scalability of analytical solutions are comprehensively verified by combining the tensile experiments, plane strain finite element method (FEM) and extensive atomistic simulations. The considerable underestimate of stretchability (e.g., >8% relatively) and overestimate of stiffness (e.g., >5% relatively) are found in some representative kirigami geometries, which show quantitative insights into the thermal effects on mechanical responses. Furthermore, several demonstrations present the developed model can be employed to enable optimization design of ribbon-kirigami-patterned conductors under the thermal effect and practical geometry constraint for searching effectively the most stretchable ribbon kirigami structures.

This paper is organized as follows. Section 2 illustrates the geometry of ribbon kirigami and describes the analytical model of normalized stiffness and stretchability using Castigliano's theorem, Moore Integral method, and LCCB theory. Section 3 presents the analysis of the underlying relationships between thermal effects, geometric effects and mechanical responses, using the developed model, FEM and available model without thermal effects. Accuracy and scalability verification of developed model are also demonstrated in this section. Section 4 describes the designing of the maximum normalized stretchability considering the thermal effects and practical geometry constraints. The concluding remarks are drawn in Section 5.

2. Establishment of analytical model

The key unit cell design of ribbon kirigami is combining with three parts: the arm section with length of l, the connection section with length of m, the curved section (arc) with arc angle of α and radius of R, as detailed in Fig. 1b, which consequently forms an unidimensional periodic ribbon kirigami structure (see the similar configuration in Fig. 1a). Utilizing dimensional analysis approach, four dimensionless parameters, the ribbon width/radius $\bar{\omega} = \omega/R$, the arm length/radius $\bar{l} = l/R$, the connection length/radius $\bar{m} = m/R$ and arc angle α, can be designated to characterize its different geometries. In particular, the ribbon kirigami becomes a straight ribbon when $\alpha = -\pi/2$.

To initiate the theoretical analysis with thermal effects, we consider a plane strain model, which suppresses its lateral buckling, and then a unit cell, using the configuration symmetry, can be straightforward represented by one quarter of the ribbon kirigami structure without the connection section. As seen in Fig. 1c, the left end of simplified model is clamped, and its right end is free but undergoes a force $F/2$ and a moment M_0. Subsequently, a homogeneous thermal load (i.e., constant temperature difference) is applied to the model, which renders a resultant force F^{th} and a moment M_0^{th} with thermal effects.

According to Fig. 1b, the non-dimensionalization length $\bar{L} = L/R$ of a unit cell of ribbon kirigami can be given in terms of the three dimensionless parameters ($\bar{l}$,$\bar{m}$ and α), as follows [32]:

$$\bar{L}/2 = \bar{m} + \cos\alpha - \bar{l}\sin\alpha \tag{1}$$

where $\bar{L} = 2(\bar{m} + \bar{l})$ if $\alpha = -\pi/2$. And the corresponding load-displacement (F' and u'_{app}) relation for this straight ribbon can be calculated by

$$u'_{app}/F' = \bar{L}/E\bar{\omega} \tag{2}$$

where $E = \bar{E}/(1-\bar{\mu}^2)$ is plane strain modulus, $\bar{E}$ is Young's modulus and $\bar{\mu}$ is Poisson's ratio.

We consider the normalized stiffness of ribbon kirigami for the case excluding thermal loading and it can be defined as $\bar{k}_{eff} = Fu'_{app}/F'u_{app}$. According to our previous work [32], the normalized stiffness $\bar{k}_{eff}$ of ribbon kirigami can be given directly using the following relation:

$$\bar{k}_{eff} = \frac{80J\bar{\omega}^2\left(24J\bar{l} + (\pi+2\alpha)\bar{\omega}^2\right)Z_1}{\begin{bmatrix}480J^2\bar{l}^4 + 480J\bar{l}^2\bar{\omega}^2 + 1872J^2\bar{l}^2\bar{\omega}^2 + 1920J^2\bar{l}\bar{m}\bar{\omega}^2 + 480J\bar{l}\pi\bar{\omega}^2 + 696J^2\bar{l}\pi\bar{\omega}^2 \\ +80J\bar{l}^3\pi\bar{\omega}^2 + 960J\bar{l}\alpha\bar{\omega}^2 + 1392J^2\bar{l}\alpha\bar{\omega}^2 + 160J\bar{l}^3\alpha\bar{\omega}^2 - 40\bar{\omega}^4 + 80J\bar{\omega}^4 - 40J^2\bar{\omega}^4 \\ +98J\bar{l}\pi\bar{\omega}^4 + 80J\bar{m}\pi\bar{\omega}^4 + 10\pi^2\bar{\omega}^4 + 29J\pi^2\bar{\omega}^4 + 196J\bar{l}\alpha\bar{\omega}^4 + 160J\bar{m}\alpha\bar{\omega}^4 + 40\pi\alpha\bar{\omega}^4 \\ +116J\pi\alpha\bar{\omega}^4 + 40\alpha^2\bar{\omega}^4 + 116J\alpha^2\bar{\omega}^4 + 2\cos 2\alpha Z_2 + \bar{\omega}^2\sin 2\alpha Z_3\end{bmatrix}} \tag{3}$$

where

$$Z_1 = \bar{L}/2 \tag{4a}$$

$$Z_2 = \begin{pmatrix}-20\bar{\omega}^4 + 40\bar{\omega}^2 + 4J^2\left(60\bar{l}^4 + 114\bar{l}^2\bar{\omega}^2 - 5\bar{\omega}^4\right) \\ +J\bar{\omega}^2\left(240\bar{l}^2 + 40\bar{l}^3(\pi+2\alpha) + \bar{l}(\pi+2\alpha)\left(29\bar{\omega}^2 - 120\right)\right)\end{pmatrix} \tag{4b}$$

$$Z_3 = \left(216J^2\bar{l} - 10(\pi+2\alpha)\bar{\omega}^2 + J\left(720\bar{l} + 240\bar{l}^2(\pi+2\alpha) + 49(\pi+2\alpha)\bar{\omega}^2\right)\right) \tag{4c}$$

$$J = 1 - \bar{\omega}/\ln\left((2+\bar{\omega})/(2-\bar{\omega})\right) \tag{4d}$$

where J represents the effect of large curvature curved beam (LCCB) on normalized stiffness of ribbon kirigami. Then the combination of Eqs. (2), (3) and Eq. (4) gives the following expression for solving the force F:

$$F = \bar{k}_{eff}E\bar{\omega}\varepsilon_1 \tag{5}$$

Then the insertion of Eqs. (5) and (7) into Eq. (6) gives the following relationship:

$$F^{th} = \bar{k}_{eff}E\bar{\omega}\left(\varepsilon_1 - \varepsilon_2\right) \tag{9}$$

Combining Eqs. (5)–(7) and (9), the normalized stiffness with thermal loading $\bar{k}'$ can be given by

$$\bar{k}' = \bar{k}_{eff}\left(1 - \varepsilon_2/\varepsilon_1\right) \tag{10}$$

According to the LCCB theory and free-body diagram as illustrated in Fig. 1b, the internal forces of arc section (see Fig. 1a) under a resultant force F^{th} and a moment M_0^{th} with thermal effects (i.e., thermal strain ε^t) can be calculated using the following relationship:

$$\begin{cases}M_{arc}^{th} = F^{th}R(1-\cos\theta)/2 - M_0^{th} \\ V_{arc}^{th} = F^{th}\sin\theta/2 \\ N_{arc}^{th} = F^{th}\cos\theta/2\end{cases} \tag{11}$$

The corresponding internal forces with thermal effects in arm section can be determined as follows:

$$\begin{cases}M_{arm}^{th} = F^{th}[R(1+\sin\alpha) + s\cos\alpha]/2 - M_0^{th} \\ V_{arm}^{th} = F^{th}\cos\alpha/2 \\ N_{arm}^{th} = -F^{th}\sin\alpha/2\end{cases} \tag{12}$$

where in Eqs. (11) and (12) M, V and N are the internal moment of the cross section, the internal shear force and the internal normal force at the centroid, respectively.

Based on the Castigliano's theorem and boundary condition $\theta_{arc}(\theta = 0) = 0$ (see Fig. 1b and c), we provide the following relationship for determining the unknown M_0^{th}:

$$\frac{M_0^{th}}{F^{th}} = \frac{\begin{pmatrix}AI\pi R + 2A\varepsilon^{th}IR\alpha + 2IS\sin\left(\left(1+\varepsilon^{th}\right)(\pi/2+\alpha)\right) - 2AIR\sin\left(\left(1+\varepsilon^{th}\right)(\pi/2+\alpha)\right) \\ +A\left(l+\varepsilon^{th}\right)^2l^2S\cos\alpha + 2A\left(1+\varepsilon^{th}\right)lRS\sin\alpha + A\varepsilon^{th}I\pi R + 2AlRS + 2A\varepsilon^{th}lRS + 2AIR\alpha\end{pmatrix}}{2A\left(1+\varepsilon^{th}\right)(2lS + I(\pi+2\alpha))} \tag{13}$$

where $\varepsilon_1 = 2u_{app}/\bar{L}$ and $\bar{k}_{eff}$ is provided in Eq. (3) to Eq. (4). To further derive the kirigami-patterned thermal loading closed-form expression of normalized stiffness, here we distinguish the contributions from mechanical loading F and non-mechanical loading $F_{non-mech}^{th}$ induced by thermal strain:

$$F^{th} = F - F_{non-mech}^{th} \tag{6}$$

For the linear superposition in Eq. (6), the non-mechanical loading contribution is subtracted from the mechanical contribution, as the positive signed mechanical strain and thermal strain can cause an opposite direction force [38]. The non-mechanical loading $F_{non-mech}^{th}$ induced by thermal strain, as listed in Eq. (6), can be expressed as the multiple of a thermal loading stiffness with the strain under thermal loading, as follows:

$$F_{non-mech}^{th} = \bar{k}_{eff}E\bar{\omega}\varepsilon_2 \tag{7}$$

where $\varepsilon_2 = (\bar{L}^{th} - \bar{L})/\bar{L}$ and $\bar{L}^{th}$ is the non-dimensionalization length of ribbon kirigami unit cell when the configuration is free to expand under thermal effects, and is given by

$$\begin{aligned}&\bar{L}^{th}/2 = \cos\left(\left(1+\varepsilon^{th}\right)(\pi/2+\alpha) - \pi/2\right) \\ &-\bar{l}\left(1+\varepsilon^{th}\right)\sin\left(\left(1+\varepsilon^{th}\right)(\pi/2+\alpha) - \pi/2\right) + \bar{m}\left(1+\varepsilon^{th}\right)\end{aligned} \tag{8}$$

where $\varepsilon^{th} = \lambda\Delta T$ is the thermal strain induced by a constant temperature difference ΔT, and λ represents the linear thermal expansion coefficient.

where $A = \omega$ is the area of cross section, $I = \omega^3/12$ is the second-area moment of the cross section, and $S = J\bar{\omega}$ represents the static moment of the cross section on neutral axis. Here, the Moore Integral method is designated to solve the applied displacement under the thermal loading u_{app}^{th}, we get

$$u_{app}^{th} = 2\delta_{arc}^{th} + 2\delta_{arm}^{th} + \delta_{connection}^{th} \tag{14}$$

where

$$\delta_{arc}^{th} = \int_0^{s^{th}}\begin{pmatrix}M_{arc}^{th}\bar{M}_{arc}^{th}/ESR + N_{arc}^{th}\bar{M}_{arc}^{th}/EAR + \\ M_{arc}^{th}\bar{N}_{arc}^{th}/EAR + N_{arc}^{th}\bar{N}_{arc}^{th}/EA + \kappa V_{arc}^{th}\bar{V}_{arc}^{th}/GA\end{pmatrix}ds_1 \tag{15}$$

$$\delta_{arm}^{th} = \int_0^{l^{th}}\left(N_{arm}^{th}\bar{N}_{arm}^{th}/EA + \kappa V_{arm}^{th}\bar{V}_{arm}^{th}/GA + M_{arm}^{th}\bar{M}_{arm}^{th}/EI\right)ds_2 \tag{16}$$

$$\delta_{connection}^{th} = \int_0^{m^{th}} N_{connection}^{th}\bar{N}_{connection}^{th}/2EA\,dl \tag{17}$$

where G is the shear modulus, κ is the correction coefficient s^{th} and l^{th} are arc length considering the thermal effects, $\bar{M}$, $\bar{V}$ and $\bar{N}$ are internal forces when $F^{th} = 1$, respectively.

Furthermore, the hoop stress in arc section using LCCB theory can be calculated by

$$\sigma = M_{arc}^{th}y/(1+y/r)\int_A\left(y^2/(1+y/r)\right)dA + N_{arc}^{th}/A \tag{18}$$

where $r/R = (1 - J) = \bar{r}$. After applying the physical equation, the maximum tension strain with thermal effects can be determined, as follows:

$$\varepsilon_{max}^{th} = -M_0^{th}(1 - \bar{\omega}/2 - \bar{r})/SE(1 - \bar{\omega}/2) + F^{th}/2EA \tag{19}$$

where M_0^{th} has been given in Eq. (13).

The current investigation involves analyzing two important mechanics indexes: the normalized stiffness and normalized stretchability. Here, the normalizes stretchability with thermal effects $\bar{\varepsilon}'$ can be defined using a continued equality [32], i.e.

$$\bar{\varepsilon}' = \varepsilon_{app}^{th}/\varepsilon_{mat}^{th} = \varepsilon_{app}^{th}/\varepsilon_{max}^{th} \tag{20}$$

where $\varepsilon_{app}^{th} = 2u_{app}^{th}/L^{th}$, ε_{max}^{th}, ε_{app}^{th} and ε_{mat}^{th} are the applied strain, the maximum strain of ribbon kirigami, the elastic stretchability and intrinsic failure strain of material, respectively. And the failure criterion is given by $\varepsilon_{max}^{th} = \varepsilon_{mat}^{th}$. For brittle materials, such as silicon we investigated in Section 3.3, ε_{mat}^{th} represents the corresponding intrinsic rupture strain.

Combination of Eqs. (1), (3), (8) and (10), the first key objective towards the normalized stiffness with thermal effects is to derive the non-dimensional functional forms of

$$\bar{k}' = \Omega\left(\alpha, \bar{l}, \bar{\omega}, \bar{m}, \varepsilon^{th}\right) \tag{21}$$

Equally, the non-dimensional functional forms of the normalized stretchability with thermal effects $\bar{\varepsilon}'$ can be expressed as follows:

$$\bar{\varepsilon}' = \Gamma\left(\alpha, \bar{l}, \bar{\omega}, \bar{m}, \varepsilon^{th}\right) \tag{22}$$

where the closed-form solutions with respect to the normalized stiffness Eq. (21) and normalized stretchability Eq. (22) are provided in Appendix. In particular, if the temperature difference $\Delta T = 0$, the non-dimensional closed-form solution in Eq. (22) (and Eq. (A2)) has been degenerated into the normalized stretchability with thermal effect absent [32]:

$$\bar{\varepsilon} = \frac{\begin{bmatrix} 480J^2\bar{l}^4 + 480J\bar{l}^2\bar{\omega}^2 + 1872J^2\bar{l}^2\bar{\omega}^2 + 1920J^2\bar{l}\bar{m}\bar{\omega}^2 + 480J\bar{l}\pi\bar{\omega}^2 + 696J^2\bar{l}\pi\bar{\omega}^2 \\ +80J\bar{l}^3\pi\bar{\omega}^2 + 960J\bar{l}\alpha\bar{\omega}^2 + 1392J^2\bar{l}\alpha\bar{\omega}^2 + 160J\bar{l}^3\alpha\bar{\omega}^2 - 40\bar{\omega}^4 + 80J\bar{\omega}^4 - 40J^2\bar{\omega}^4 \\ +98J\bar{l}\pi\bar{\omega}^4 + 80J\bar{m}\pi\bar{\omega}^4 + 10\pi^2\bar{\omega}^4 + 29J\pi^2\bar{\omega}^4 + 196J\bar{l}\alpha\bar{\omega}^4 + 160J\bar{m}\alpha\bar{\omega}^4 + 40\pi\alpha\bar{\omega}^4 \\ +116J\pi\alpha\bar{\omega}^4 + 40\alpha^2\bar{\omega}^4 + 116J\alpha^2\bar{\omega}^4 + 2\cos 2\alpha Z_2 + \bar{\omega}^2 \sin 2\alpha Z_3 \end{bmatrix}}{\left(40\bar{\omega}^2 Z_1/(2 - \bar{\omega})\right)\begin{bmatrix} (1 - J)\bar{\omega}\left(24J\bar{l} + (\pi + 2\alpha)\bar{\omega}^2\right) \\ -2(2J - \bar{\omega})\left(-\bar{\omega}^2 + J\left(6\bar{l}^2 + \bar{\omega}^2\right)\right)\cos\alpha \\ -24J\bar{l}(2J - \bar{\omega})\sin\alpha \end{bmatrix}} \tag{23}$$

where Z_1, Z_2, Z_3 and J are provided in Eq. (4).

And up to now, we have provided the closed-form expressions that characterize the mechanical responses in relation to the normalized stiffness and stretchability to homogeneous thermal loading. However, Effects of temperature difference on mechanical responses of ribbon kirigami in Eqs. (21) and (22) are difficult to ascertain, because of extreme complexity. To unveil the underlying relations between thermal effects, mechanical responses and geometric effects, two relative errors$\delta_{stiffness}$ and $\delta_{stretchability}$ are introduced, and thermal effects on the normalized stiffness and stretchability will be quantitatively explored and compared, as we conducted in Section 3, using Eqs. (3), (21), (22), (23) and the following expressions

$$\delta_{stiffness} = \left|\left|\bar{k}_{eff}\right| - |\bar{k}'|\right|/|\bar{k}'| \tag{24}$$

$$\delta_{stretchability} = ||\bar{\varepsilon}| - |\bar{\varepsilon}'||/|\bar{\varepsilon}'| \tag{25}$$

Furthermore, finite element method (FEM) is carried out with the use of ABAQUS software to validate the model. The simulation model exploits plane strain elements with refined meshes to model the ribbon kirigami structures with various geometries. The material attribute is assumed to be polymer, with elastic modulus of 0.5 MPa, Poisson's ratio of 0.4 and thermal expansion coefficient of 340×10^{-6} °C^{-1} [39]. Nominal strain of 0.02 is externally applied to the ribbon kirigami structures. As a homogeneous thermal loading, a constant temperature difference of 50 °C is designated although we investigate different temperature differences.

3. Results and discussion

3.1. Thermal effect on the normalized stiffness and stretchability

Fig. 2 reveals the results of the normalized stiffness and corresponding stretchability with three temperature differences ΔT = 50K,150K,300K for geometries $\bar{\omega} = 0.2$, $\bar{m}$=0, $\bar{l}$=1, 3 and different levels of α. The developed thermal loading closed-form expressions show great agreement with the FEM results. However, the results emerging from the model with and without thermal effects indicate that the significant discrepancies exist among the curves with different temperature differences. As a demonstration, as detailed in Fig 2b, the thermal absent model gives the stretchability of 17.23 for $\bar{\omega} = 0.2$, $\bar{m}$=0, $\bar{l}$=3 and $\alpha = -0.28$, which is 31% smaller than that of developed model $\bar{\varepsilon}' = 24.95$ at a temperature difference of 300 °C. In practical applications, such as kirigami-patterned bioprobes for experiments in vitro of myocardium [9], the similar underestimation of stretchability is dangerous and fatal.

Based on Eqs. (24) and (25), Fig. 3 provides the quantitative insights with respect to $\delta_{stiffness}$ and $\delta_{stretchability}$ into the thermal effects (ΔT = 50K) on mechanical responses. Because of geometry effects, the relationships between $\delta_{stiffness}$, $\delta_{stretchability}$ and three varying dimensionless parameters are illustrated in Fig. 3a and d. Through assigning the value of $\bar{\omega} = 0.2$, the dependencies of $\delta_{stiffness}$ and $\delta_{stretchability}$ on $\bar{l}$ and α are unveiled in Fig. 3b and e. With increasing of $\bar{l}$ (see Fig. 3a and d) for specific $\bar{\omega}$, α, $\bar{m}$ and ΔT, $\delta_{stiffness}$ (up to ~ 5%) and $\delta_{stretchability}$ (up to ~ 8%) increase dramatically, which is a direct consequence of long arm effect [32] that larger arm length will magnify the effective length with thermal strain. Fig. 3b and e confirm these findings, but for a specific $\bar{l}$ with the increasing of α from −1.0 to 1.0 $\delta_{stiffness}$ decreases (see Fig. 3b).

While for the relative error of normalized stretchability the corresponding $\delta_{stretchability}$ is increasing for the same geometries (see Fig. 3e). Fig. 3c and f demonstrate the evolutions of $\delta_{stiffness}$ and $\delta_{stretchability}$ with the increasing of $\bar{\omega}$. G_1, G_2, G_3, g_1, g_2, and g_3 correspond to the representative geometric points in Fig. 3b and e. For these ribbon kirigami structures, $\delta_{stretchability}$ is insensitive to the variation of $\bar{\omega}$. For relatively short ribbon kirigami (see G_1), $\delta_{stiffness}$ decreases monotonously if $\bar{\omega}$ is increasing, but it changes to be insensitive when arm length is large (see G_2 and G_3). Taking $\bar{l} = 5$ in Fig. 3c and f as an example, $\delta_{stiffness}$ and $\delta_{stretchability}$ are about 4% and 6.7%, indicating that the normalized stiffness and stretchability are considerable overestimateand and underestimate, respectively. Therefore, the thermal effects and resultant errors are non-negligible in applications [10,22,24,27].

3.2. Effect of geometry parameters on ribbon kirigami with thermal loading

As demonstrated in Section 3.1, as α varies in a wide range, thermal effect (or thermal loading) will lower the normalized stiffness and heighten the normalized stretchability of ribbon kirigami throughout its whole process from "insensitive" regime to "loading" regime. Here, we start by revealing the effects of constant temperature differences on mechanical responses of ribbon kirigami structures, combining with systematic geometric parameter effects including α, $\bar{\omega}$, $\bar{l}$ and $\bar{m}$.

The geometry effects regarding four independent dimensionless parameters on the normalized stiffness with and without considering

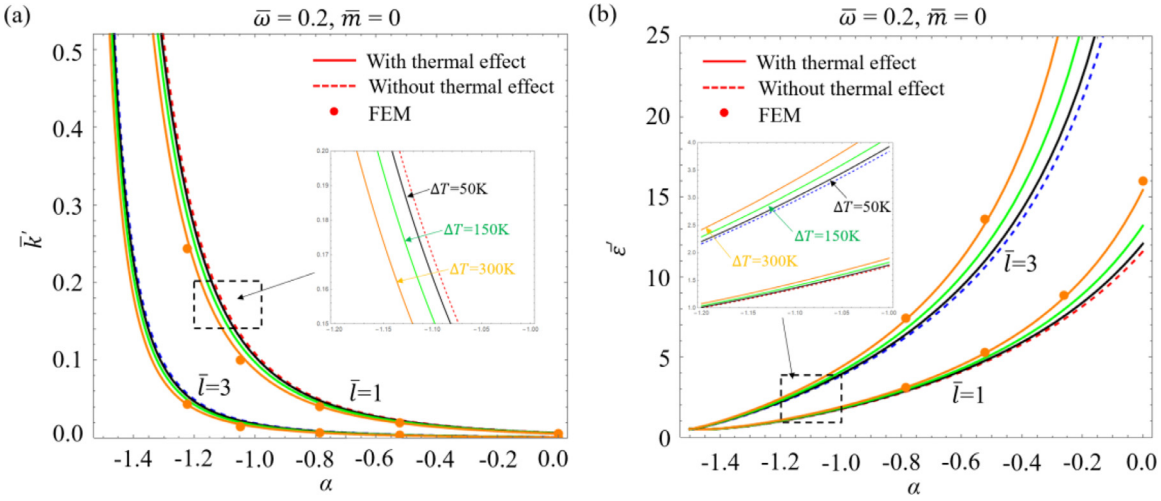

Fig. 2. The analytical and FEM results of (a) the normalized stiffness and (b) the normalized stretchability with thermal effect (i.e., $\Delta T = 50$K, 150K, 300K) and without thermal effect for $\bar{\omega} = 0.2$, $\bar{m}$=0 and $\bar{l}$=1, 3 under different levels of α.

thermal loadings are clearly illustrated in Fig. 4a–c. The predictions from developed model agree remarkably well with the plane strain FEM results for various representative geometries, which demonstrate the monotonic patterns, that is, the normalized stiffness $\bar{k}'$ could be lowered by increasing $\bar{l}$, α and reducing $\bar{\omega}$. Comparing Fig. 4a–c, while $\bar{\omega}$, $\bar{l}$, and α, for a specific geometry, are all monotonic, but the constant temperature differences apply to kirigami configurations in a similar approach, which render the overestimate of normalized stiffness. Especially, with the increasing of $\bar{\omega}$ thermal effects will "load" the normalized stiffness significantly, as evident from Fig. 4a. In the case of $\alpha = 0$, $\bar{m} = 0$, $\bar{\omega} = 1$ and $\bar{l} = 0$, the relative error regarding the normalized stiffness is $\delta_{stiffness}$=7.7%, indicating the larger $\bar{\omega}$ could lead to larger contribution of thermal loading with $\bar{l}$ absent. This effect can also be found in Fig. 3a where is represented by the counterintuitive red zone. Therefore, we advocate that kirigami-geometry-patterned design of stretchable conductors should be carefully performed, and the influence of thermal effects cannot be neglected in practical applications.

Fig. 4d–f reveal the effects of geometric parameters on normalized stretchability with and without thermal loadings by using Eqs. (22), (23) and FEM. In general, the analytical solutions according to Eq. (22) show great agreement with the FEM results, and the theoretical models with and without thermal effects and FEM results are plotted as the solid lines, dashed lines and filled circles, respectively. As can be seen from Fig. 4d and e, normalized stretchability $\bar{\varepsilon}'$ is always larger than 1 for the wide range of $\bar{m}$, $\bar{\omega}$ and $\bar{l}$, which signifies the promising capacity for ribbon-kirigami-based design towards the variable geometrical structure patterns presents a desirable approach in decreasing the intrinsic tension strain with thermal loading [32,40,41]. The contribution of geometry-dependent effect on enhancement of stretchability for kirigami is consistent with previous experimental results, including those for hybrid kirigami-patterned metamaterials [17], kirigami skins [5], and programmable kirigami metastructures [37]. Furthermore, it is evident from the Fig. 4d and e that typical evolutions of $\bar{\varepsilon}'$ for the increasing of $\bar{\omega}$ and $\bar{l}$ are monotonic but present an opposite tendency, that is, $\bar{\varepsilon}'$ with thermal effects increases as $\bar{l}$ increases but it increases with the decreasing of $\bar{\omega}$. However, for practical applications, the larger $\bar{l}$ and the smaller $\bar{\omega}$ sometimes would restrict the device performance of kirigami-based stretchable conductor, such as stretchable bioprobe [9] and wearable thermotherapy [10], etc., also it is impossible to achieve the extreme sizes of ribbon kirigami due to the technical bottlenecks regarding resolution restriction of photolithography [40]. To response such a significant problem, we considering the thermal effects and practical geometric restraint conditions perform the design optimization towards the most stretchable ribbon kirigami conductor, as detailed in Section 4. Fig. 4f provides the comparison of two different models and FEM results for $\bar{\omega} = 0.2$, $\bar{l} = 3$, and $\bar{m} = 0, 2, 4, 6, 8, 10$, respectively. For relatively short $\bar{m}$ (such as $\bar{m} = 0, 2$), $\bar{\varepsilon}'$ increases dramatically as α, while it first increases followed by a slight drop for relatively large $\bar{m}$ (see $\bar{m} = 8, 10$). The limited regime of α, resulting in $\bar{\varepsilon}' < 1$, is not conducive to enhance the normalized stretchability with thermal effects according to Eq. (20), which indicates the previous ribbon-kirigami-patterned design depending on experience cannot always enable a reliable guide in increasing the stretchability. Comparing Fig. 4d–f, it is clear that distinct "loading" regime and "insensitive" regime of monotonic $\bar{\varepsilon}'$ exist, for a wide range of variation in geometric parameters. Towards the thermal effect (or loading) on normalized stretchability, it is thought that the larger $\bar{l}$, the smaller $\bar{m}$ and the larger α would "load" the normalized stretchability $\bar{\varepsilon}'$ more. We should note that the relatively error of normalized stretchability, for the kirigami configuration $\alpha = 0$, $\bar{\omega} = 0.5$, $\bar{m} = 0$, $\bar{l} = 5$, could be as many as $\delta_{stretchability}$=15.9% as evident in Fig. 4e. Moreover, the ribbon width/radius $\bar{\omega}$ in Fig. 4d and the arc angle α in Fig. 4f should be precisely controlled in ribbon kirigami design, because of relative complexity of "loading" regime and "insensitive" regime from geometry effect. Of course, the knowledge of developed thermal loading closed-form solutions regarding Eqs. (21) and (22) and quantitative characterizations with regard to the relative errors of normalized stiffness and stretchability in Figs. 2 and 3 can serve as an important guide in speed-up of designing the desirable ribbon kirigami conductor devices. In short, the remarkable underestimate of stretchability and overestimate of stiffness can be induced by the thermal-effect-absent model, the more accurate predictions we developed of ribbon kirigami considering the practical conditions would be helpful in rational selection and design optimization of kirigami-based devices in applications.

3.3. Experimental verification

3.3.1. Experiment evaluation

Fig. 5a reveals the comparison of developed model and thermal-effect-absent model based on Eqs. (22) and (23) and experimental data according to different representative geometries. All ribbon kirigami structures are manufactured by ultraviolet (UV) post-cured polymer with temperature of glass transition Tg = 62 °C and coefficient of thermal expansion 95×10^{-6} °C^{-1} ($T <$ Tg). The ribbon width and ribbon thickness are respectively designated as 1 mm and 10 mm, which suppress the lateral buckling of ribbon kirigami structures. Concretely speaking, the 3D-printed ribbon kirigami structure is first placed into temperature

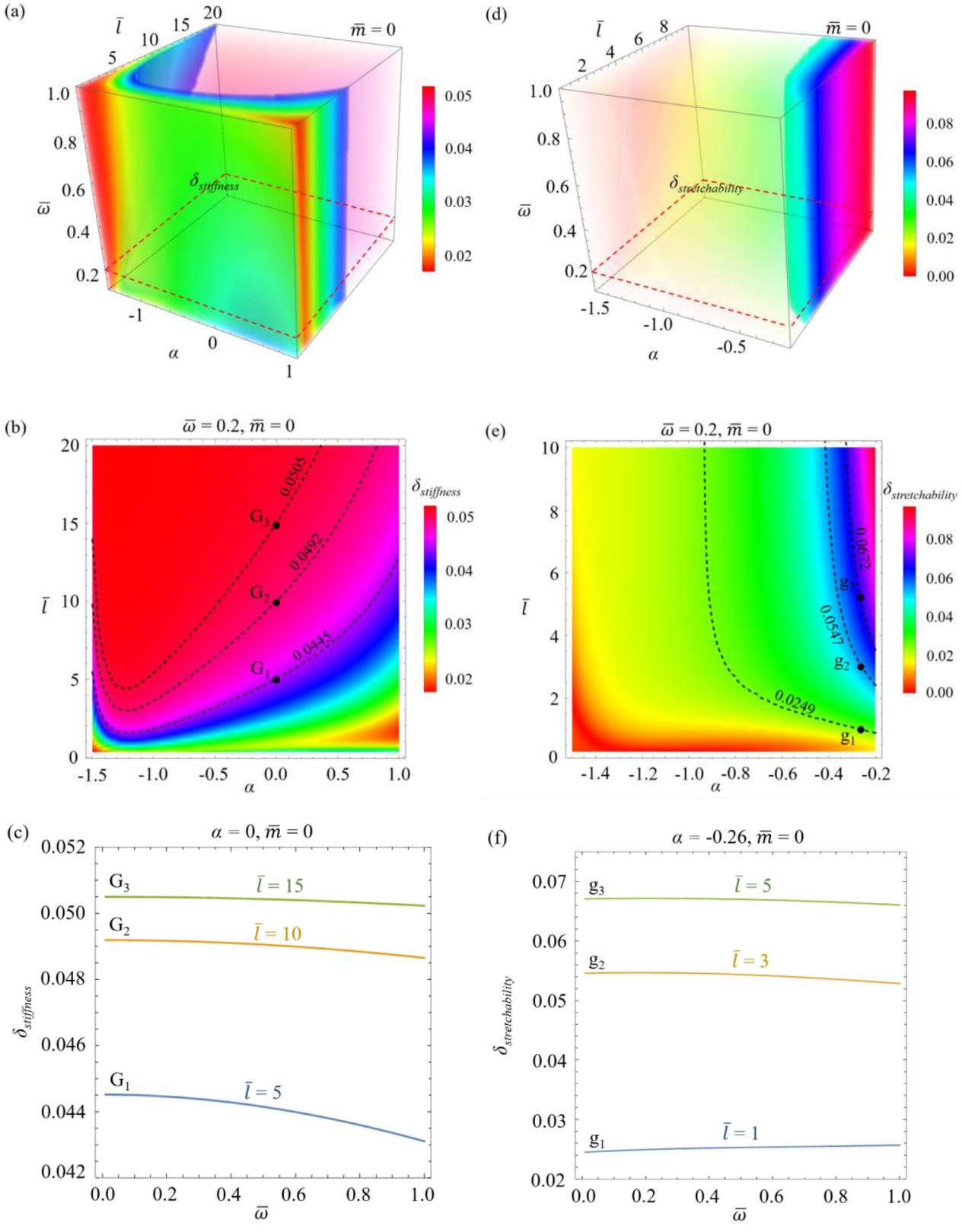

Fig. 3. Relative errors of the normalized stiffness between two different theoretical models for (a) geometries with $\bar{m}$=0 and various α, $\bar{\omega}$, $\bar{l}$ and (b) geometries with $\bar{\omega}$ = 0.2, $\bar{m}$=0 and various α, $\bar{l}$. (c) Relative errors of representative geometries G_1, G_2 and G_3 in Fig. 3b under different levels of $\bar{\omega}$. (d–f) The Corresponding results for relative errors of the normalized stretchability.

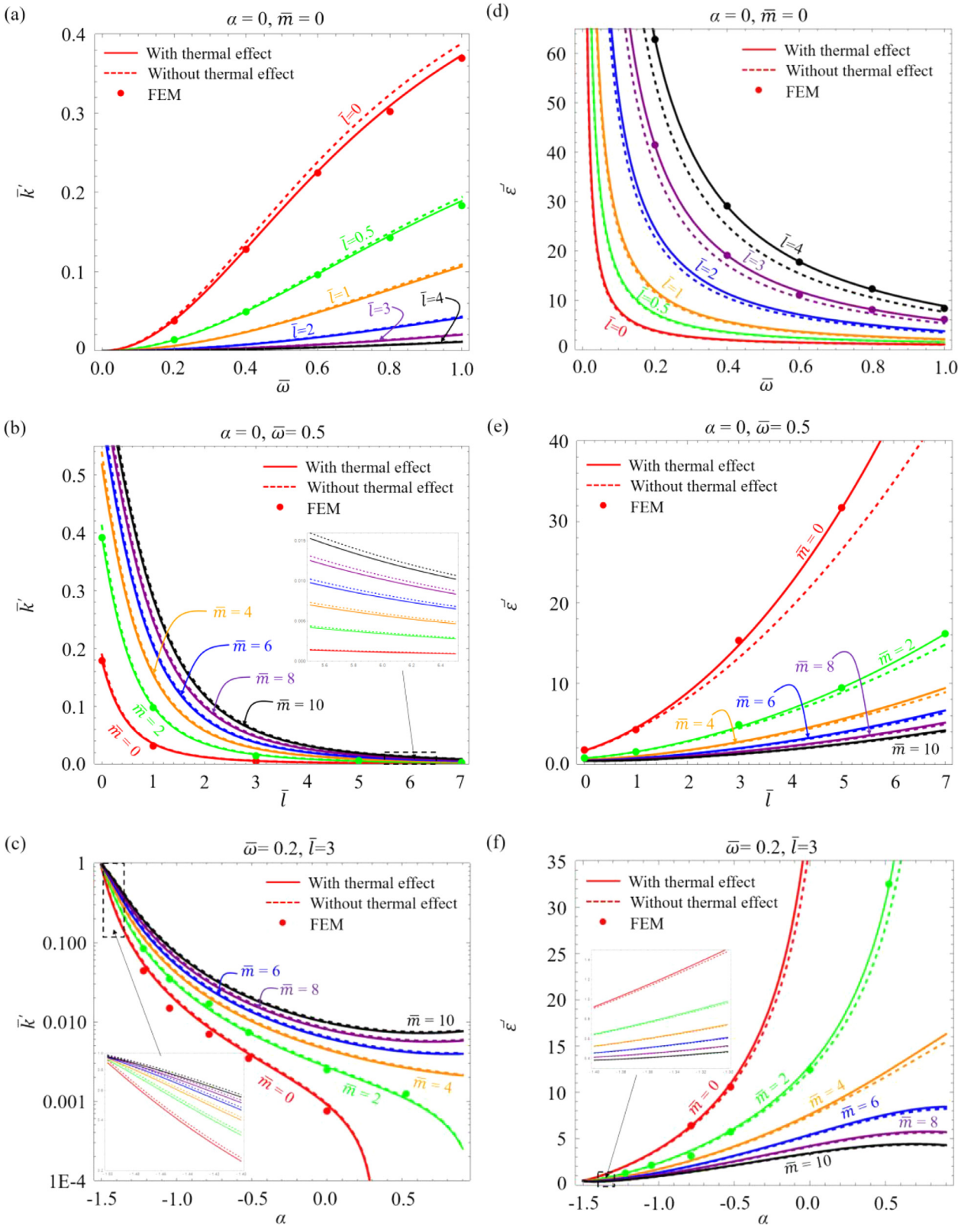

Fig. 4. Schematic illustration of the normalized stiffness with and without thermal effects of ribbon kirigami structures, with geometric parameters of $\alpha = 0$, $\bar{m} = 0$, $\bar{l} = 0, 0.5, 1, 2, 3, 4$ in (a), $\alpha = 0$, $\bar{\omega} = 0.5$, $\bar{m} = 0, 2, 4, 6, 8, 10$ in (b), and α, $\bar{\omega} = 0.2$, $\bar{l} = 3$, $\bar{m} = 0, 2, 4, 6, 8, 10$ in (c). (d-f) Similar results for the normalized stretchability of ribbon kirigami structures.

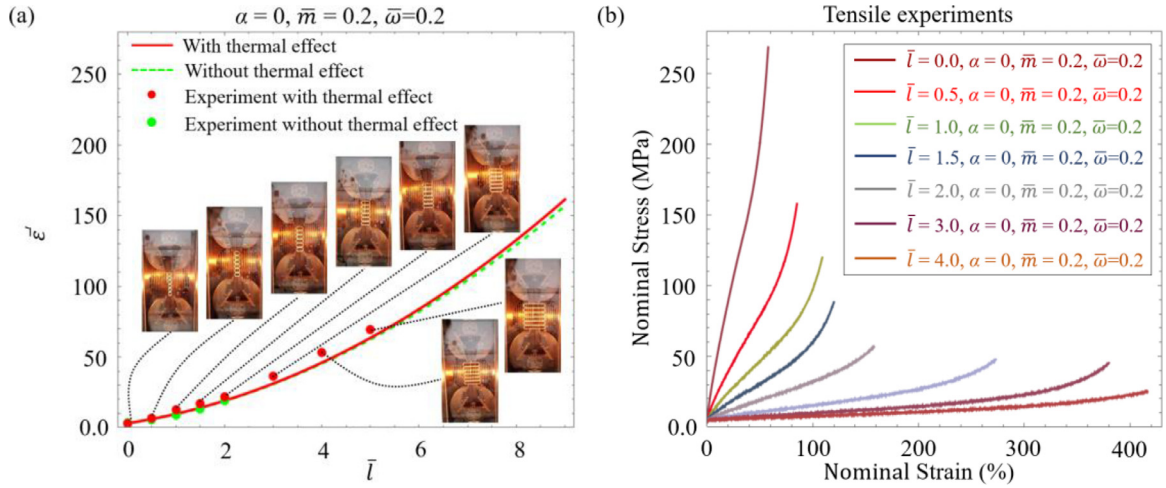

Fig. 5. (a) Experimental results and theoretical predictions with and without thermal effects for ribbon kirigami structures $\alpha = 0$, $\bar{m} = 0.2$, and $\bar{\omega} = 0.2$. (b) The corresponding stress-strain curves of 3D-printed ribbon kirigami structures.

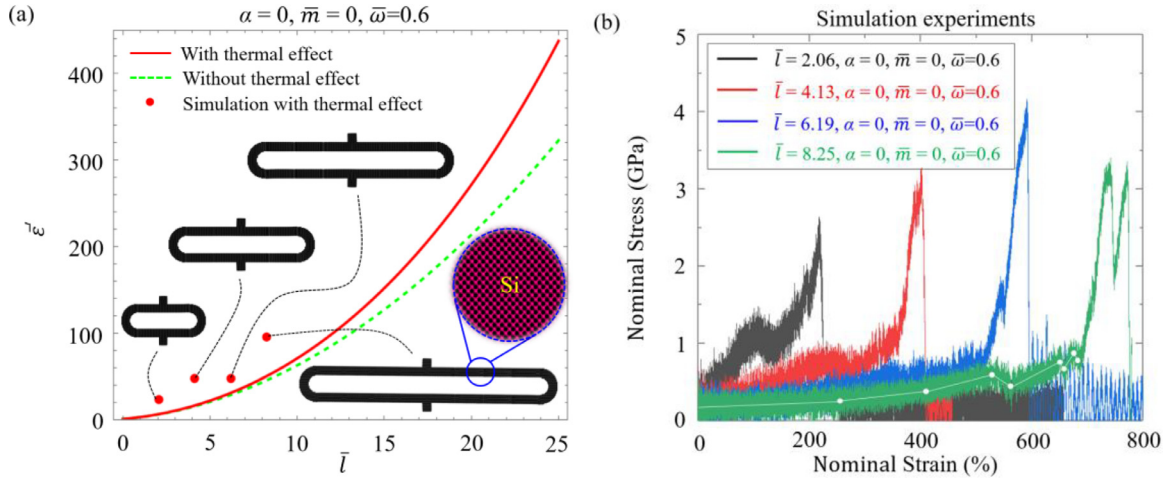

Fig. 6. (a) Atomistic simulation results and theoretical predictions with and without thermal effects for low dimension silicon ribbon kirigami nano-structures with geometries $\alpha = 0$, $\bar{m} = 0$, $\bar{\omega} = 0.60$ and $\bar{l} = 2.06, 4.13, 6.19, 8.25$. (b) The corresponding stress-strain curves of silicon kirigami nano-structures.

box of tensile experimental system to allow it expanding freely under the constant temperature difference of 22 °C (up to 45 °C and 300 s), and then it is carefully clamped with antiskid at this stable temperature. A strain ratio of 0.01 s^{-1} is applied to produce the exact stress-strain curve combining INSTRON 5965, US. According to Eq. (20), we evaluate the strain towards the LCCB beam and straight beam, separately. The normalized elastic stretchability is achieved using different representative ribbon kirigami configurations, and the intrinsic failure strain (i.e., 5%) of kirigami is carefully obtained using configuration $\alpha = -\pi/2$. Fig. 5b illustrates the experimental stress-strain curves at different strain levels. Combining Fig. 5a and b, it is somewhat surprising to see that the normalized stretchability with thermal effect for experimental results shows remarkable agreement with the developed closed-form solution, which can be attributed to the rational introduction of thermal effect, effective application of LCCB theory and energy methods. These observations directly demonstrate that our theory modeling with practical thermal effect consideration can provide insights into the design and application of ribbon kirigami structures.

3.3.2. *Model scalability*

It is important to note that expressions of the developed models regarding normalized stiffness and stretchability are non-dimensionalization (such as $\bar{\varepsilon}' = \Gamma(\alpha, \bar{l}, \bar{\omega}, \bar{m}, \varepsilon^{th})$). Therefore, if we neglect the size-dependent effect of materials the mechanical model of ribbon kirigami structures with the specific geometry, no matter macro- and nano-scale, is scalable. To investigate the model scalability of ribbon kirigami, the extensive atomistic simulation experiments are carried out using the Large-scale Atomic-Molecular Massively Parallel Simulator (LAMMPS) code package developed by Sandia National Laboratories [42]. The Erhart/Albe-Tersoff potential is designated to describe the interactions of silicon atoms for low dimension silicon kirigami nano-structures, which is in line with our previous works [32,43]. Throughout the experimental process, a simulation system containing a silicon kirigami with width 17.33 Å and thickness 21.72 Å is established and periodic boundary condition is applied to the direction of thickness, which simulate the plane strain model in current research. To stabilize the silicon kirigami nano-structures generated by in-house code, all silicon kirigami constructions are first quasi-statically optimized using the Conjugated-Gradient (CG) algorithm. Simulation experiments are performed in the NVE ensemble with a constant temperature 1500 K, and the thermal expansion coefficient is about 4.26×10^{-6} K^{-1} [44]. The Berendsen thermostat is employed to control the temperature. Standard velocity-Verlet integration algorithm is used in current research to integrate the equations of motion. The time step is set to be 1fs. After that, the displacement loadings of 0.02 nm/ps is used on the right connection end of silicon kirigami while left end is fixed. Fig. 6b illustrates

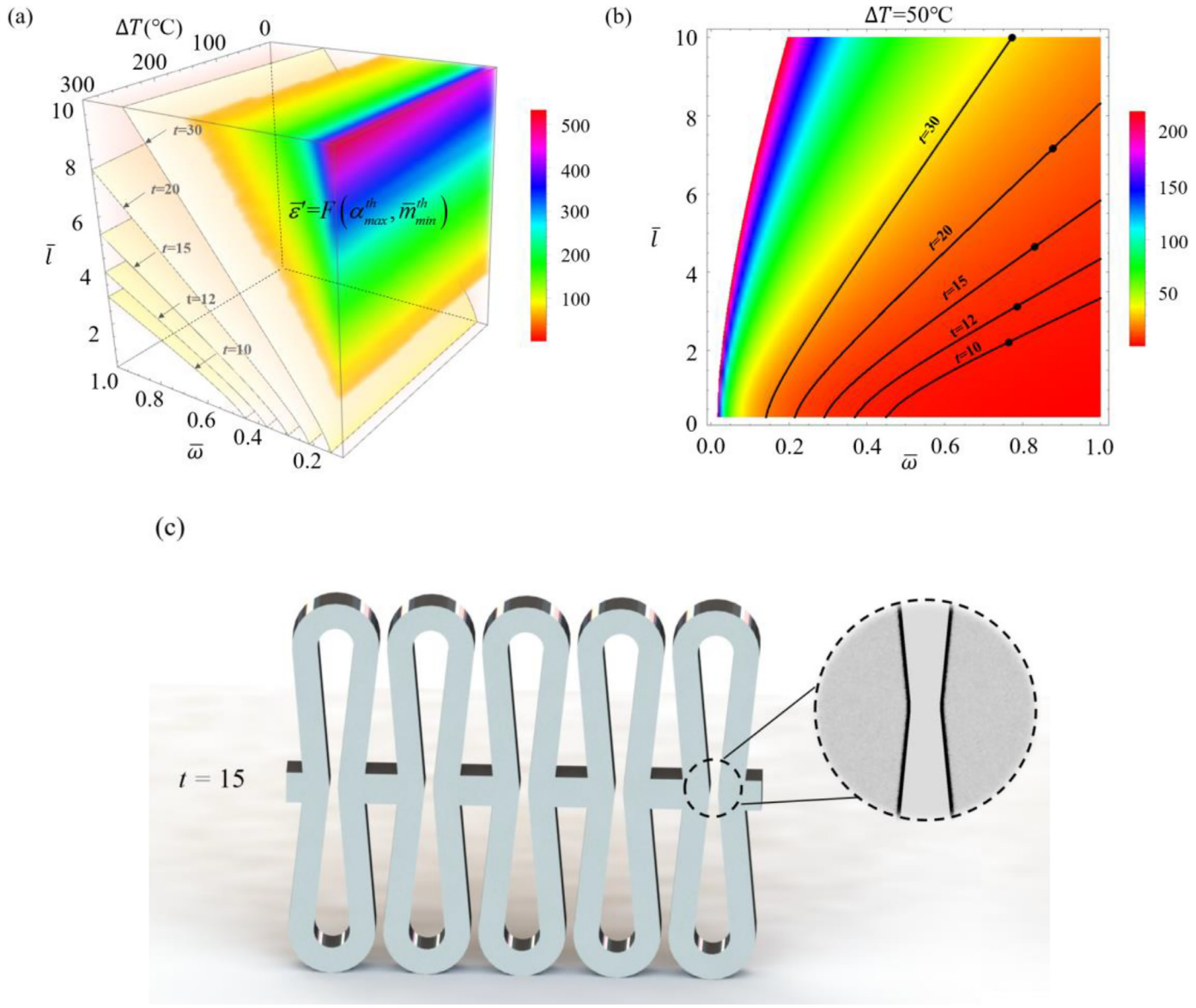

Fig. 7. (a) Schematic illustration of distribution with regard to $\bar{\omega}$, $\bar{l}$ and ΔT, which can be plotted by $\bar{\varepsilon}'=F(\alpha_{max}^{th},\bar{m}_{min}^{th})$. (b) Distribution of the normalized stretchability for $\bar{\omega}$ and $\bar{l}$, the constant temperature difference is designated as 50 °C. (c) The ribbon kirigami configuration with the most normalized stretchability when $t=15$, $\bar{\omega}=0.831$, $\bar{l}=4.655$, $\bar{m}=0.993$ and $\alpha=0.096$.

the experimental stress-strain curves for different representative silicon kirigami nano-structures with geometries $\alpha=0$, $\bar{m}=0$, $\bar{\omega}=0.60$ and $\bar{l}=2.06, 4.13, 6.19, 8.25$, based on which the normalized elastic stretchability can be determined carefully. Fig. 6a reveals the comparison of normalized elasticity stretchability with and without thermal effects and atomistic simulation results, the predictions are in agreement with the extensive atomistic simulation experiments, while we ignore the size effect in low dimensional silicon material. We should note that the dimensionless parameters for the unit cell of ribbon kirigami to derive all the equation is a general step for the solution procedure. However, in the small system, there is definitely a size effect that cannot just be explained with non-dimensionalization. For example, as the size of the systems becomes small, the surface-to-volume ratio increases and surface effect will be dominant, and the heat loss from the heater will be increased due to the increased surface area for convection heat transfer. Future work should be devoted to systematic investigation of properties evaluation of kirigami structures with size effects. Moreover, in light of high performance of high-quality inorganic electronic materials especially for silicon in modern electronics, we anticipate special care of low dimension silicon kirigami could be taken.

4. Optimization considering practical geometry constraints and thermal effects

In practical applications, ribbon-kirigami-patterned stretchable conductors tend to undergo the action of Joule heating effect and geometry constant conditions. In particular, (a) the non-overlapped conditions should be used in one-directional periodic kirigami structures to guarantee the physical rationality; (b) in-plane breadth conditions can be utilized either in optically and thermally correlated sensors to maintain the device performance, or in highly stretchable novel physical devices with regard to kirigami configurations to break through the limitation of resolution of photolithography to obtain the maximum stretchability. Based on our thermal loading closed-form theoretical model and geometry characterizations of ribbon kirigami, we perform the design

Table 1
The geometric parameters after design optimization for the maximum stretchability of ribbon kirigami structures.

t	$\bar{\omega}$	$\bar{l}$	$\bar{m}$	α
10	0.765	2.211	0.993	0.236
12	0.786	3.126	0.993	0.160
15	0.831	4.655	0.993	0.096
20	0.878	7.163	0.993	0.050
30	0.772	9.993	0.994	0.034

optimization with practical geometry constraints and thermal effects of ribbon kirigami in this section.

Firstly, non-overlapped conditions can be correlated to L_1 and L_2, as detailed in Fig. 1b. After applying the non-dimensionalization process and homogeneous temperature difference, the non-overlapped conditions regarding $\overline{L}_1^{th}$ and $\bar{L}_2^{th}$ can be calculated in terms of five dimensionless parameters ($\bar{\omega}$, $\bar{l}$, $\bar{m}$, α and ε^{th}), as follows:

$$\overline{L}_1^{th} = 1 - \bar{\omega}/2 - \begin{pmatrix} (1-\bar{\omega}/2)\left(1-\cos\left(\left(1+\varepsilon^{th}\right)(\alpha+\pi/2)-\pi/2\right)\right) \\ +\bar{l}\left(1+\varepsilon^{th}\right)\sin\left(\left(1+\varepsilon^{th}\right)(\alpha+\pi/2)-\pi/2\right) \\ +\bar{\omega}/2\left(1-\cos\left(\left(1+\varepsilon^{th}\right)(\alpha+\pi/2)-\pi/2\right)\right) \end{pmatrix} \tag{26}$$

$$\bar{L}_2^{th} = \bar{m}\left(1+\varepsilon^{th}\right) - \begin{pmatrix} \bar{l}\sin\left(\left(1+\varepsilon^{th}\right)(\alpha+\pi/2)-\pi/2\right)+\bar{\omega}/2 \\ +\left(1-\cos\left(\left(1+\varepsilon^{th}\right)(\alpha+\pi/2)-\pi/2\right)\right) \end{pmatrix} \tag{27}$$

Then, values of α_{max}^{th} and $\bar{m}_{min}^{th}$ according to Eqs. (26) and (27) ($0 \le \overline{L}_1^{th}$ and $0 \le \bar{L}_2^{th}$) can be given using the following relationships

$$\alpha_{max}^{th} = \left(-\pi\varepsilon^{th} + 4\arctan\left(\left(-2\bar{l} + \sqrt{4\bar{l}^2+4-\bar{\omega}^2}\right)/2+\bar{\omega}\right)\right)/2\left(1+\varepsilon^{th}\right) \tag{28}$$

$$\bar{m}_{min}^{th} = \begin{pmatrix} 2+\bar{\omega}-2\left(1+\varepsilon^{th}\right)\bar{l}\cos\left(\left(1+\varepsilon^{th}\right)(\alpha+\pi/2)\right) \\ -2\sin\left(\left(1+\varepsilon^{th}\right)(\alpha+\pi/2)\right) \end{pmatrix}/2\left(1+\varepsilon^{th}\right) \tag{29}$$

Secondly, the dimensionless $\bar{L}_3$ in relation to in-plane breadth condition can be defined, and in-plane breadth considering the thermal effect $\bar{L}_3^{th}$ can be calculated by

$$\begin{aligned} \bar{L}_3^{th}/2 = t\bar{\omega}/2 = 1+\bar{\omega}/2+\sin\left((\pi/2+\alpha)\left(1+\varepsilon^{th}\right)-\pi/2\right) \\ +\bar{l}\left(1+\varepsilon^{th}\right)\cos\left((\pi/2+\alpha)\left(1+\varepsilon^{th}\right)-\pi/2\right) \end{aligned} \tag{30}$$

where t, a scaling factor, represents the in-plane breadth of ribbon kirigami is t times larger than that of ribbon width. Next combination of Eqs. (28)–(30) and (22) gives the normalized stretchability $\bar{\varepsilon}'$ as the function of α_{max}^{th} and $\bar{m}_{min}^{th}$, as follows:

$$\bar{\varepsilon}' = F\left(\alpha_{max}^{th}, \bar{m}_{min}^{th}\right) \tag{31}$$

where $\bar{\varepsilon}' = F(\alpha_{max}^{th}, \bar{m}_{min}^{th})$ is characterized in Fig. 7a and b. Utilizing the Eq. (30), the normalized stretchability under constant temperature difference and geometry constraints can be determined numerically with a sufficient accuracy. This process can be realized by using the commercial software MATLAB.

Finally, according to the numerical calculation results represented by the black dots in Fig. 7b, the optimized geometric parameters of $\bar{\omega}$ and $\bar{l}$ can be obtained. Next, with the $\bar{\omega}$, $\bar{l}$, Eqs. (28) and (29) in hand, all of representative geometry parameters leading to the maximum stretchability can be determined, as we provided in Table 1. As a demonstration, Fig. 7c illustrates the corresponding geometric configuration with the maximum stretchability when $t = 15$ and $\Delta T = 50$ °C. We should note that the design optimization method we used here is in line with the Lagrangian multiplier method, but it can serve as an important technology in speed-up of searching the optimal solutions because of conciseness and practicability. Finally, for the potential applications with respect to kirigami-based stretchable electronics, we advocate that designs of stretchable kirigami conductors encompassing Joule heating effects by experience should be carefully performed. And the developed analytical models with some counterintuitive expectations can be used to guide the rational selection of design variables to design the novel devices through high parallel mechanical-physical process.

5. Conclusions

The theoretical model of ribbon kirigami considering thermal effect and large curvature curved beam (LCCB) theory has been developed toward the applications of highly stretchable conductor devices. Thermal loading closed-form solutions regarding the key mechanics indexes of normalized stiffness and stretchability have been presented, which their excellent accuracy and scalability have been validated using tensile experiments, thermal-absent theoretical model, plane strain FEM, and atomistic simulation. Especially, thermal loading effects combining with comprehensively dimensionless geometry parameters on normalized stiffness and stretchability are systematically and quantitatively demonstrated based on introduced relative errors. This study reveals that significant "insensitive" state and "loading" state exist in normalized stiffness and stretchability when ribbon kirigami structures undergo a homogeneous temperature difference. Monotonic $\bar{\varepsilon}'$ and $\bar{k}'$ show an opposite evolution tendency with increasing of $\bar{\omega}$ and $\bar{l}$ (or α), indicating that combination of thermal effects and variable geometric effects can increase normalized stretchability and decrease normalized stiffness by several orders of magnitude except for some unexpected results. In addition, the larger $\bar{l}$ could carry more thermal effects on mechanical responses of ribbon kirigami structures, resulting in a remarkably relative error (e.g., 15.9%) compared to thermal-absent model. The obtained results show that considerable underestimate of stretchability (e.g., >8% relatively) and overestimate of stiffness (e.g., >5% relatively) can be dangerous in practical applications. And considering effects of constant temperature differences is of great important for kirigami design optimization, based on which the maximum normalized stretchability can be obtained using developed theoretical model and geometric constant consideration. In short, this paper provides a foundational study to serve as a guideline for the design of ribbon-kirigami-patterned stretchable conductors.

Declaration of Competing Interest

The authors declared that they have no conflicts of interest to this work.

Acknowledgments

This work was supported by National Natural Science Foundation of China, 11572099 and 11872160. The author wishes to thank Mrs. Zaiying Zhang and Mr. Gongran Wang for their thoughtful kindness. The author would like to express his thanks to the editor and anonymous reviewers whose constructive comment significantly improved the paper.

Appendix

The expressions of $\bar{k}' = \Omega(\alpha, \bar{l}, \bar{\omega}, \bar{m}, \varepsilon^{th})$ and $\bar{\varepsilon}' = \Gamma(\alpha, \bar{l}, \bar{\omega}, \bar{m}, \varepsilon^{th})$ in Eqs. (21) and (22) are given by

$$\bar{k}' = \frac{80X_3J\bar{\omega}^2(24J\bar{l}+\pi\bar{\omega}^2+2\alpha\bar{\omega}^2)(\bar{m}+\cos\alpha-\bar{l}\sin\alpha)}{\begin{bmatrix} X_1480J^2\bar{l}^4+X_2352J^2\bar{l}^2\bar{\omega}^2+X_21920J^2\bar{l}\bar{m}\bar{\omega}^2+X_2480J\bar{l}\pi\bar{\omega}^2 \\ +X_2696J^2\bar{l}\pi\bar{\omega}^2+X_180J\bar{l}^3\pi\bar{\omega}^2+X_2960J\bar{l}\alpha\bar{\omega}+X_21392J^2\bar{l}\alpha\bar{\omega} \\ +X_1160J\bar{l}^3\alpha\bar{\omega}^2+X_640\bar{\omega}^4+X_298J\bar{l}\pi\bar{\omega}^4+X_280J\bar{m}\pi\bar{\omega}^4+X_210\pi^2\bar{\omega}^4 \\ +X_229J\pi^2\bar{\omega}^4+X_2196J\bar{l}\alpha\bar{\omega}^4+X_2160J\bar{m}\alpha\bar{\omega}^4+X_240\pi\alpha\bar{\omega}^4 \\ +X_2116J\pi\alpha\bar{\omega}^4+X_240\alpha^2\bar{\omega}^4+X_2116J\alpha^2\bar{\omega}^4+Y_1\cos2\alpha+Y_2\cos\left(\varepsilon^{th}X_5/2\right) \\ -X_640\bar{\omega}^4\cos\left(X_3(\pi+2\alpha)\right)+Y_3960\cos\left(\alpha+X_3X_5/2\right)+Y_4\sin2\alpha \\ +Y_5\sin\left(\varepsilon^{th}X_5/2\right)+Y_6\sin\left(X_3X_5\right)+Y_7\sin\left(\alpha+X_3X_5/2\right) \end{bmatrix}} \tag{A1}$$

$$\bar{\varepsilon}' = \frac{\begin{bmatrix} X_1480J^2\bar{l}^4 + X_22352J^2\bar{l}^2\bar{\omega}^2 + X_21920J^2\bar{l}\bar{m}\bar{\omega}^2 + X_2480J\bar{l}\pi\bar{\omega}^2 \\ +X_2696J^2\bar{l}\pi\bar{\omega}^2 + X_180J\bar{l}^3\pi\bar{\omega}^2 + X_2960J\bar{l}\alpha\bar{\omega} + X_21392J^2\bar{l}\alpha\bar{\omega} \\ +X_1160J\bar{l}^3\alpha\bar{\omega}^2 + X_640\bar{\omega}^4 + X_298J\bar{l}\pi\bar{\omega}^4 + X_280J\bar{m}\pi\bar{\omega}^4 + X_210\pi^2\bar{\omega}^4 \\ +X_229J\pi^2\bar{\omega}^4 + X_2196J\bar{l}\alpha\bar{\omega}^4 + X_2160J\bar{m}\alpha\bar{\omega}^4 + X_240\pi\alpha\bar{\omega}^4 \\ +X_2116J\pi\alpha\bar{\omega}^4 + X_240\alpha^2\bar{\omega}^4 + X_2116J\alpha^2\bar{\omega}^4 + Y_1\cos 2\alpha + Y_2\cos\left(\varepsilon^{th}X_5/2\right) \\ -X_640\bar{\omega}^4\cos\left(X_3(\pi+2\alpha)\right) + Y_3960\cos\left(\alpha + X_3X_5/2\right) + Y_4\sin 2\alpha \\ +Y_5\sin\left(\varepsilon^{th}X_5/2\right) + Y_6\sin\left(X_3X_5\right) + Y_7\sin\left(\alpha + X_3X_5/2\right) \end{bmatrix}}{\frac{40\bar{\omega}^2\begin{pmatrix} X_3\bar{m} + \sin\left(X_3X_5/2\right) \\ +X_3\bar{l}\cos\left(X_3X_5/2\right)\end{pmatrix}}{2-\bar{\omega}}\begin{pmatrix} X_324J\bar{l}\bar{\omega} - X_324J^2\bar{l}\bar{\omega} + X_3\pi\bar{\omega}^3 - X_3J\pi\bar{\omega}^3 \\ +X_32\alpha\bar{\omega}^3 - X_32J\alpha\bar{\omega}^3 \\ +\left(-X_224J^2\bar{l}^2 + X_212J\bar{l}^2\bar{\omega}\right)\cos\alpha \\ +\left(-X_348J^2\bar{l} + X_324J\bar{l}\bar{\omega}\right)\sin\alpha \\ +\left(4J\bar{\omega}^2 - 4J^2\bar{\omega}^2 - 2\bar{\omega}^3 + 2J\bar{\omega}^3\right)\sin\left(X_3X_5/2\right)\end{pmatrix}} \tag{A2}$$

where

$$X_1=\left(1+4\varepsilon^{th}+6\left(\varepsilon^{th}\right)^2+4\left(\varepsilon^{th}\right)^3+\left(\varepsilon^{th}\right)^4\right) \tag{A3}$$

$$X_2=\left(1+2\varepsilon^{th}+\left(\varepsilon^{th}\right)^2\right) \tag{A4}$$

$$X_3=\left(1+\varepsilon^{th}\right) \tag{A5}$$

$$X_4=\left(1+3\varepsilon^{th}+3\left(\varepsilon^{th}\right)^2+\left(\varepsilon^{th}\right)^3\right) \tag{A6}$$

$$X_5=(\pi+2\alpha) \tag{A7}$$

$$X_6=\left(-1+2J-J^2\right) \tag{A8}$$

$$Y_1=\begin{pmatrix} X_1480J^2\bar{l}^4 + X_21392J^2\bar{l}^2\bar{\omega}^2 - X_2240J\bar{l}\pi\bar{\omega}^2 + X_180J\bar{l}^3\pi\bar{\omega}^2 \\ -X_2480J\bar{l}\alpha\bar{\omega}^2 + X_1160J\bar{l}^3\alpha\bar{\omega}^2 + X_258J\bar{l}\pi\bar{\omega}^2 + X_2116J\bar{l}\alpha\bar{\omega}^4 \end{pmatrix} \tag{A9}$$

$$Y_2=\left(X_2480J\bar{l}^2\bar{\omega}^2 - X_2480J^2\bar{l}^2\bar{\omega}^2\right) \tag{A10}$$

$$Y_3=\left(-X_3J\bar{l}\bar{\omega}^2 + X_3J^2\bar{l}\bar{\omega}^2\right) \tag{A11}$$

$$Y_4=\left(X_4240J\bar{l}^2\pi\bar{\omega}^2 + X_4480J\bar{l}^2\alpha\bar{\omega}^2\right) \tag{A12}$$

$$Y_5=\left(-X_3960J\bar{l}\bar{\omega}^2 + X_3960J^2\bar{l}\bar{\omega}^2\right) \tag{A13}$$

$$Y_6=\begin{pmatrix} X_3240J\bar{l}\bar{\omega}^2 - X_31176J^2\bar{l}\bar{\omega}^2 + X_310\pi\bar{\omega}^4 \\ -X_349J\pi\bar{\omega}^4 + X_320\alpha\bar{\omega}^4 - X_398J\alpha\bar{\omega} \end{pmatrix} \tag{A14}$$

$$Y_7=\left(X_2480J\bar{l}^2\bar{\omega}^2 - X_2480J^2\bar{l}^2\bar{\omega}^2\right) \tag{A15}$$

References

[1] Sussman DM, Cho Y, Castle T, Gong X, Jung E, Yang S, et al. Algorithmic lattice kirigami: a route to pluripotent materials. PNAS 2015;112(24):7449–53.
[2] Cho Y, Shin JH, Costa A, Kim TA, Kunin V, Li J, et al. Engineering the shape and structure of materials by fractal cut. PNAS 2014;111(49):17390–5.
[3] Blees MK, Barnard AW, Rose PA, Roberts SP, McGill KL, Huang PY, et al. Graphene kirigami. Nature 2015;524(7564):204.
[4] Shyu TC, Damasceno PF, Dodd PM, Lamoureux A, Xu L, Shlian M, et al. A kirigami approach to engineering elasticity in nanocomposites through patterned defects. Nat Mater 2015;14(8):785–9.
[5] Rafsanjani A, Zhang YR, Liu BY, Rubinstein SM, Bertoldi K. Kirigami skins make a simple soft actuator crawl. Sci Robot 2018;3(15).
[6] Collins GPScience and. culture: kirigami and technology cut a fine figure, together. PNAS 2016;113(2):240–1.
[7] Rafsanjani A, Jin L, Deng B, Bertoldi K. Propagation of pop ups in kirigami shells. PNAS 2019;116(17):8200–5.
[8] Smart AG. Rewriting the rules of kirigami. Phys Today 2015;68(1):13–14.
[9] Morikawa Y, Yamagiwa S, Sawahata H, Numano R, Koida K, Ishida M, et al. Ultra-stretchable kirigami bioprobes. Adv Health Mater 2018;7(3).
[10] Jang NS, Kim KH, Ha SH, Jung SH, Lee HM, Kim JM. Simple approach to high-performance stretchable heaters based on kirigami patterning of conductive paper for wearable thermotherapy applications. ACS Appl Mater Inter 2017;9(23):19612–21.
[11] Hong S, Lee H, Lee J, Kwon J, Han S, Suh YD, et al. Highly stretchable and transparent metal nanowire heater for wearable electronics applications. Adv Mater 2015;27(32):4744–51.
[12] Xu L, Wang X, Kim Y, Shyu TC, Lyu J, Kotov NA. Kirigami nanocomposites as wide-angle diffraction gratings. ACS Nano 2016;10(6):6156–62.
[13] Wang W, Li C, Rodrigue H, Yuan F, Han MW, Cho M, et al. Kirigami/Origami-Based soft deployable reflector for optical beam steering. Adva Funct Mater 2017;27(7):1604214.
[14] Wu C, Wang X, Lin L, Guo H, Wang ZL. Paper-Based triboelectric nanogenerators made of stretchable interlocking kirigami patterns. ACS Nano 2016;10(4):4652–9.
[15] Won P, Park JJ, Lee T, Ha I, Han S, Choi M, et al. Stretchable and transparent kirigami conductor of nanowire percolation network for electronic skin applications. Nano Lett 2019;19(9):6087–96.
[16] Hu N, Chen D, Wang D, Huang S, Trase I, Grover HM, et al. Stretchable kirigami polyvinylidene difluoride thin films for energy harvesting: design, analysis, and performance. Phys Rev Appl 2018;9(2):1–6.
[17] Hwang DG, Bartlett MD. Tunable mechanical metamaterials through hybrid kirigami structures. Sci Rep 2018;8(1):3378.
[18] Chen SH, Chan KC, Yue TM, Wu FF. Highly stretchable kirigami metallic glass structures with ultra-small strain energy loss. Scrip Materialia 2018;142:83–7.
[19] Kim H, Lee H, Ha I, Jung J, Won P, Cho H, et al. Biomimetic color changing anisotropic soft actuators with integrated metal nanowire percolation network transparent heaters for soft robotics. Adv Funct Mater 2018;28(32):1801847.
[20] Suh YD, Jung J, Lee H, Yeo J, Hong S, Lee P, et al. Nanowire reinforced nanoparticle nanocomposite for highly flexible transparent electrodes: borrowing ideas from macrocomposites in steel-wire reinforced concrete. J Mater Chem C 2017;5(4):791–8.
[21] Lamoureux A, Lee K, Shlian M, Forrest SR, Shtein M. Dynamic kirigami structures for integrated solar tracking. Nat Commun 2015;6:8092.
[22] Lyu J, Hammig MD, Liu L, Xu L, Chi H, Uher C, et al. Stretchable conductors by kirigami patterning of aramid-silver nanocomposites with zero conductance gradient. Appl Phys Lett 2017;111(16):161901.
[23] Okogbue E, Han SS, Ko TJ, Chung HS, Ma J, Shawkat MS, et al. Multifunctional two-dimensional PtSe2-layer kirigami conductors with 2000% stretchability and metallic-to-semiconducting tunability. Nano Lett 2019 Will appear soon.
[24] Guan YS, Zhang Z, Tang Y, Yin J, Ren S. Kirigami-inspired nanoconfined polymer conducting nanosheets with 2000% stretchability. Adv Mater 2018;30(20):e1706390.
[25] Hwang DG, Trent K, Bartlett MD. Kirigami-Inspired structures for smart adhesion. ACS Appl Mater Inter 2018;10(7):6747–54.
[26] Ma R, Wu C, Wang ZL, Tsukruk VV. Pop-Up conducting large-area biographene kirigami. ACS Nano 2018;12(10):9714–20.
[27] Zheng W, Huang W, Gao F, Yang H, Dai M, Liu G, et al. Kirigami-Inspired highly stretchable nanoscale devices using multidimensional deformation of monolayer MoS2. Chem Mater 2018;30(17):6063–70.
[28] Wang Z, Zhang L, Duan S, Jiang H, Shen J, Li C. Kirigami-patterned highly stretchable conductors from flexible carbon nanotube-embedded polymer films. J Mater Chem C 2017;5(34):8714–22.
[29] Zhao R, Lin S, Yuk H, Zhao X. Kirigami enhances film adhesion. Soft Matter 2018;14(13):2515–25.
[30] Guan YS, Li H, Ren F, Ren S. Kirigami-inspired conducting polymer thermoelectrics from electrostatic recognition driven assembly. ACS Nano 2018;12(8):7967–73.
[31] Mortazavi B, Lherbier A, Fan Z, Harju A, Rabczuk T, Charlier JC. Thermal and electronic transport characteristics of highly stretchable graphene kirigami. Nanoscale 2017;9(42):16329–41.
[32] Wang Y, Wang C, Tan H. Geometry-dependent stretchability and stiffness of ribbon kirigami based on large curvature curved beam model. Int J Solids Struct 2020;182–183C:236–53.
[33] Rafsanjani A, Bertoldi K. Buckling-induced kirigami. Phys Rev Lett 2017;118(8):084301.

[34] Yang Y, Dias MA, Holmes DP. Multistable kirigami for tunable architected materials. Phys Rev Mater 2018;2(11):1–7.
[35] Isobe M, Okumura K. Initial rigid response and softening transition of highly stretchable kirigami sheet materials. Sci Rep 2016;6:24758.
[36] Dias MA, McCarron MP, Rayneau-Kirkhope D, Hanakata PZ, Campbell DK, Park HS, et al. Kirigami actuators. Soft Matter 2017;13(48):9087–92.
[37] Tang Y, Lin G, Yang S, Yi YK, Kamien RD, Yin J. Programmable Kiri-Kirigami metamaterials. Adv Mater 2017;29(10):1–9.
[38] Karathanasopoulos N, Ganghoffer J-F, Papailiou KO. Analytical closed-form expressions for the structural response of helical constructions to thermal loads. Int J Mech Sci 2016;117:258–64.
[39] Muller A, Wapler MC, Wallrabe U. A quick and accurate method to determine the Poisson's ratio and the coefficient of thermal expansion of PDMS. Soft Matter 2019;15(4):779–84.
[40] Lu N, Yang S. Mechanics for stretchable sensors. Curr Opin Solid State Mater Sci 2015;19(3):149–59.
[41] Zhang Y, Huang Y, Rogers JA. Mechanics of stretchable batteries and supercapacitors. Curr Opin Solid State Mater Sci 2015;19(3):190–9.
[42] Plimpton S. Fast parallel algorithms for short-range molecular-dynamics. J Comput Phys 1995;117(1):1–19.
[43] Wang Y, Wang C, Zhang Y, Tan H. Graphene kirigami as reinforcement and interfacial bonding effect for toughness and strength of silicon-based nanocomposites. Comput Mate Sci 2019;159:306–15.
[44] Tokumaru OYY. Precise determination of lattice parameter and thermal expansion coefficient of silicon between 300 and 1500 K. J Appl Phys 1984;56(2) 314-0.